PAPER

Check for updates

Fractal structured charge-excitation triboelectric nanogenerators for powering portable electronic devices†

Hairong Long,‡[a,b] Jie An,‡[b] Shuxing Xu,[a,b] Xiuhui Ni,[c,d] Erming Su,[a,b] Yingjin Luo,[b] Shijie Liu [b,e] and Tao Jiang ✶[a,b,e]

Effective power management on the outputs of triboelectric nanogenerators (TENGs) is critical for their practical applications due to the large impedance and unbalanced load matching. Recently proposed voltage multiplying circuits for external-charge excitation and self-charge excitation are usually unstable and require reversal for device restarting and common switched-capacitor-converters usually cause large switching losses. In this work, we fabricated a fractal structured charge-excitation circuit for TENGs using diodes and capacitors. The fractal switched-capacitor-converter coupled with voltage regulator diodes can greatly boost the output charge and current of the TENG without reverse starting. The managed output performance of the TENG can be controlled by the electronic component parameters and external operating frequency. Through the component and condition optimization, the fractal structured charge-excitation TENG (FSC-TENG) can achieve nearly 5.8 times charge boosting and almost 16.8 times power boosting in the pulsed mode. Furthermore, the FSC-TENG successfully drove a hygrothermograph and was integrated into a yoga mat for harvesting human-body motion energy to power an electronic watch and a pedometer. The FSC-TENG with good charge accumulation properties and stability is a promising candidate for practical self-powered applications.

Introduction

With the rapid development of portable, wearable electronic devices and Internet of Things (IoT) technologies, people's demand for mobile and distributed sustainable energy has gradually increased.[1] In the era of IoTs and big data, portable electronics for sensing,[2,3] physiological monitoring,[4] data communication,[5,6] and human–machine interaction,[7,8] *etc.*, are enriching and changing our daily lives. However, no matter how convenient they are for us, they cannot survive without

batteries for power supply.[9] Using batteries to power a large number of small electronic devices will bring huge maintenance costs and serious environmental pollution problems from waste batteries.[8,10,11] Therefore, it is urgent to seek feasible approaches for self-powering these electronic devices. Harvesting mechanical energy effectively from the ambient environment to provide electrical energy is a promising solution to attaining this goal, possibly, by means of electromagnetic,[12] electrostatic,[13] piezoelectric,[8,10,14] and triboelectric power-generation technologies.[15–18]

The triboelectric nanogenerator (TENG) invented by Prof. Wang, based on the coupling effect of triboelectrification and electrostatic induction, can effectively convert randomly-distributed, irregular, and low-frequency mechanical energy into electricity.[19] It adopts the mechanism of Maxwell's displacement current and exhibits the merits of low cost,[20,21] easy to fabricate,[22] diverse material selection,[23] and wide application range.[24] It can be applied in the fields of wearable devices,[25] smart homes,[26] and memory of electronic equipment,[27] *etc.* In order to enhance the charge density of tribo-surfaces for improving the power output of TENG toward practical applications, considerable efforts have been made through various approaches, such as material modification,[2] surface structuring,[28] charge pumping,[29,30] charge shuttling,[31] self-charge

[a]School of Chemistry and Chemical Engineering, Guangxi University, Nanning, Guangxi 530004, P. R. China
[b]CAS Center for Excellence in Nanoscience, Beijing Key Laboratory of Micro-Nano Energy and Sensor, Beijing Institute of Nanoenergy and Nanosystems, Chinese Academy of Sciences, Beijing 101400, P. R. China. E-mail: jiangtao@binn.cas.cn
[c]Shandong Technological Center of Oceanographic Instrumentation Co., Ltd, Qingdao 266001, P. R. China
[d]Institute of Oceanographic Instrumentation, QiLu University of Technology (Shandong Academy of Sciences), Qingdao 266001, P. R. China
[e]School of Nanoscience and Technology, University of Chinese Academy of Sciences, Beijing 100049, P. R. China
†Electronic supplementary information (ESI) available. See DOI: https://doi.org/10.1039/d2nr06328j
‡These authors contributed equally to this work.

excitation,[32,33] mechanical switch adjustment,[34] and multi-switch operation.[35] In 2018, a charge excitation strategy for the TENG system was proposed using a voltage multiplying circuit (VMC) to implement external-charge excitation and self-charge excitation of TENG.[33] The output performance of the TENG was significantly boosted by the VMC, but the circuit is unstable and requires reversal for device restarting when releasing the charges from the capacitors. Then, a switched-capacitor-converter based on the fractal design (FSCC) was proposed in 2019, which is equivalent to a fractal structure VMC that can lower the voltage and boost the charge and current.[36] However, it is difficult to prepare closed electronic devices due to the requirement of adding automatic switches to control the outputs. Therefore, we urgently need to overcome the above drawbacks, so that the charge excitation circuit can be used in actual situations for powering small portable electronics by the TENG.

In this work, an FSCC (fractal structured VMC) with voltage regulator diodes was developed to manage the electrical outputs of TENG, where the fractal charge-excitation circuit can realize the charge boosting without reverse starting. The influences of the electronic component parameters and external operating frequency on the output charge and current of the fractal structured charge-excitation TENG (FSC-TENG) were systematically investigated. The FSCC integrated on a printed circuit board (PCB) can boost the output charge of a common TENG by nearly 5.8 times under regular triggering, achieving a short-circuit current of 36.5 µA and a transferred charge of 752.4 nC. Then, the FSC-TENG could deliver an output power of 7.83 mW with an enhancement of about 16.8 times, which can easily drive a hygrothermograph. Furthermore, the FSC-TENG was placed underneath a yoga mat to capture human-body motion energy for powering portable electronics such as an electronic watch and a pedometer, demonstrating important application prospects of the FSC-TENG system with good charge accumulation property and stability.

Experimental section

Fabrication of the TENG

Two pieces of acrylic boards were cut into substrates with the dimensions of 100 mm × 100 mm × 5 mm using a laser cutter (PLS6.75). A foam of 100 mm × 100 mm × 5 mm with high density was fixed onto the top surface of the bottom acrylic substrate, and a Kapton film of 100 mm × 100 mm × 50 µm was attached to the upper surface of copper (Cu) electrode of 100 mm × 100 mm × 25 µm. Another substrate was attached by a layer of Cu electrode.

Fabrication of the FSCC

For the FSCC integrated on a breadboard, the diode models used in the different FSCCs were 1N4004, 1N4005, BYV26D, 1N4007, and R3000, whose corresponding breakdown voltages were 400 V, 600 V, 800 V, 1000 V, and 3000 V, respectively, and the leakage current was 5 µA. The FSCCs were installed on the

breadboard with the sizes of 35 mm × 47 mm. For the FSCC integrated on the PCB, the model of surface-mounted diodes was 1N4007, and the package specifications for SMD diode and capacitors were 1206. The breakdown voltage for the 1 nF, 10 nF, and 22 nF capacitors was 2 kV, while that for the 100 nF capacitor was 1 kV. The PCB circuit diagram was designed by Altium Designer, and the PCB proofing patches were completed by commercial factories.

Electrical measurements

The contact-separation process of the TENG was driven by a linear motor. The output voltage, current, and transferred charge of the TENG were measured using a current preamplifier (Keithley 6514 System Electrometer).

Results and discussion

An FSCC was built to integrate with a contact-separation mode TENG, forming a fractal structured charge-excitation TENG, as schematically shown in Fig. 1a. The FSC-TENG with a size of 100 mm × 100 mm was based on the contact electrification between 25 µm-thick copper (Cu) electrode and a 50 µm-thick Kapton film attached to another copper electrode, which photograph is shown in ESI Fig. S1.† A flexible sponge was sandwiched between the Kapton-Cu film and acrylic substrate for improving the material contact intimacy. The FSCC adopts the fractal structure of 4 = 2 × 2 (2nd order 4-unit), having 9 rectifier diodes and 4 identical ceramic capacitors. This circuit could only use high-voltage ceramic capacitors, and ordinary commercial capacitors with low withstand voltage were not applicable. The device and circuit fabrication process can be found in the Experimental section. The entire circuit system of the FSCC with a Zener diode for the TENG is depicted in Fig. 1b. The connection manner of the capacitor group can automatically switch between parallel and series, leading to constant variation in the overall voltage of the capacitor group, and the charge excitation is realized during the contact separation process. A Zener diode was used to regulate the voltage and avoid dielectric breakdown. Fig. 1c is a simple schematic diagram of the electronic elements, and the system achieves a current output by the charge transfer between the TENG and ceramic capacitors under the action of unidirectional diodes.

Fig. 1d–i shows the working principle for the FSC-TENG system. At the initial state, there are no charges stored in the four capacitors (Fig. 1d). Here, the TENG acted as a voltage source (voltage V is applied to the FSCC) and the connection manner of capacitors in the FSCC can automatically switch between the series and parallel. When the tribo-pair in the TENG was separated, the electrostatic charges are transferred to the FSCC, as shown in Fig. 1e. Along the red line, the input charge Q flows across the capacitors in series, and each capacitor has a charge Q and the voltage of $V/4$. When the TENG was into a contact state again, the decrease in voltage V resulted in the charge transfer from the capacitors to the TENG (Fig. 1f). The capacitor connection was automatically switched to be in
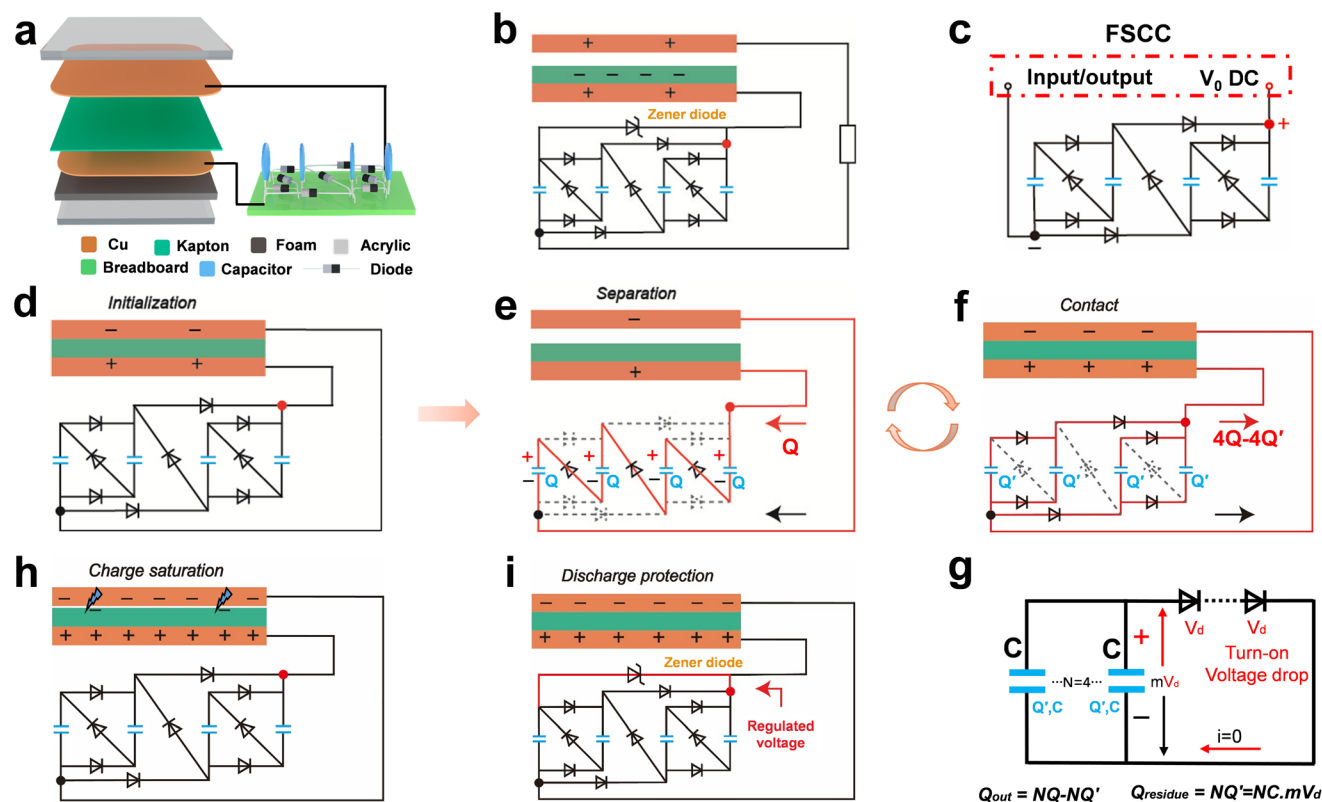
Fig. 1 Working principle of the fractal structured charge-excitation TENG. (a) Schematic illustration of the FSC-TENG with an FSCC of 4 = 2 × 2 structure. (b) Whole circuit system of the FSCC with a Zener diode for the FSC-TENG. (c) Input/output node and scheme of the FSCC. (d) Charge distribution of FSC-TENG at the initial state. (e–g) Charge-excitation process during periodic contact-separation cycles. (h and i) Schematic charge distribution in the FSC-TENG at the (h) charge saturation, and (i) discharge protection using a regulator diode.

parallel, due to the unidirectional conductivity of the diodes. The output charge of $4Q-4Q'$ and the voltage of $V/4-2V_d$ were released and fed back to the TENG, where Q' and $2V_d$ are the charge and total output voltage drop, retained in each capacitor because of the turn-on voltage drop of the diodes, and V_d is the voltage drop of one diode. The equivalent circuit of the discharge process of an N-unit FSCC consists of N capacitors in parallel and m diodes in series, resulting in the total output voltage drop of mV_d and residue charge of $NC \cdot mV_d$ (Fig. 1g). The output charge released from the FSCC is $NQ-NC \cdot mV_d$, in which, $N = 4$ for this work. After several cycles, the charges flow back to the TENG until the charge saturation (Fig. 1h), where further charge excitation may induce the air breakdown. To ensure stable output, a regulator diode was used to control the voltage and thus release excessive charges (Fig. 1i).

To verify the functionality of the FSC-TENG system, the output performance of the TENG was systematically tested and compared for the two cases with and without charge excitation (Fig. 2a) under regular triggering of the linear motor. The moving distance of the linear motor was fixed at 14 cm, and the frequency was set to 1 Hz in the tests. When the common TENG was directly connected to the linear motor, the short-circuit current and transferred charge of the TENG were only 3.5 μA and 110.0 nC, respectively (Fig. 2b and c). On the other

hand, for the FSC-TENG, with an FSCC consisting of 9 rectifier diodes, 4 ceramic capacitors, and voltage regulator diodes, the short-circuit current and transferred charge of the TENG reach saturation values after 25 s (Fig. 2d and e), which were 36.5 μA and 752.4 nC, respectively. However, it was found that the outputs were unstable without the regulator diodes (ESI Fig. S2a and b†), which is related to the fractal structure of the self-excitation circuit itself. Appropriate regulated voltage was chosen to ensure the output stability of the TENG. The voltage output of the TENG with/without the charge excitation is shown in ESI Fig. S3.† In addition, in order to study whether the FSCC can be re-charged after discharging, we discharged the capacitors and then re-measured the outputs of TENG at 1 Hz, as shown in Fig. 2f and g. It can be seen that the short-circuit current and transferred charge can increase again until they get saturated. ESI Video S1† records the recharging process after the discharging process at a frequency of 1 Hz, and the corresponding transferred charge profile of the FSC-TENG is shown in ESI Fig. S4.† The fractal charge-excitation circuit improves the output performance of the TENG, and the matched regulator diode can maintain and stabilize the maximum outputs to a certain extent, during the charging and discharging process, which again verifies the good stability of this circuit.
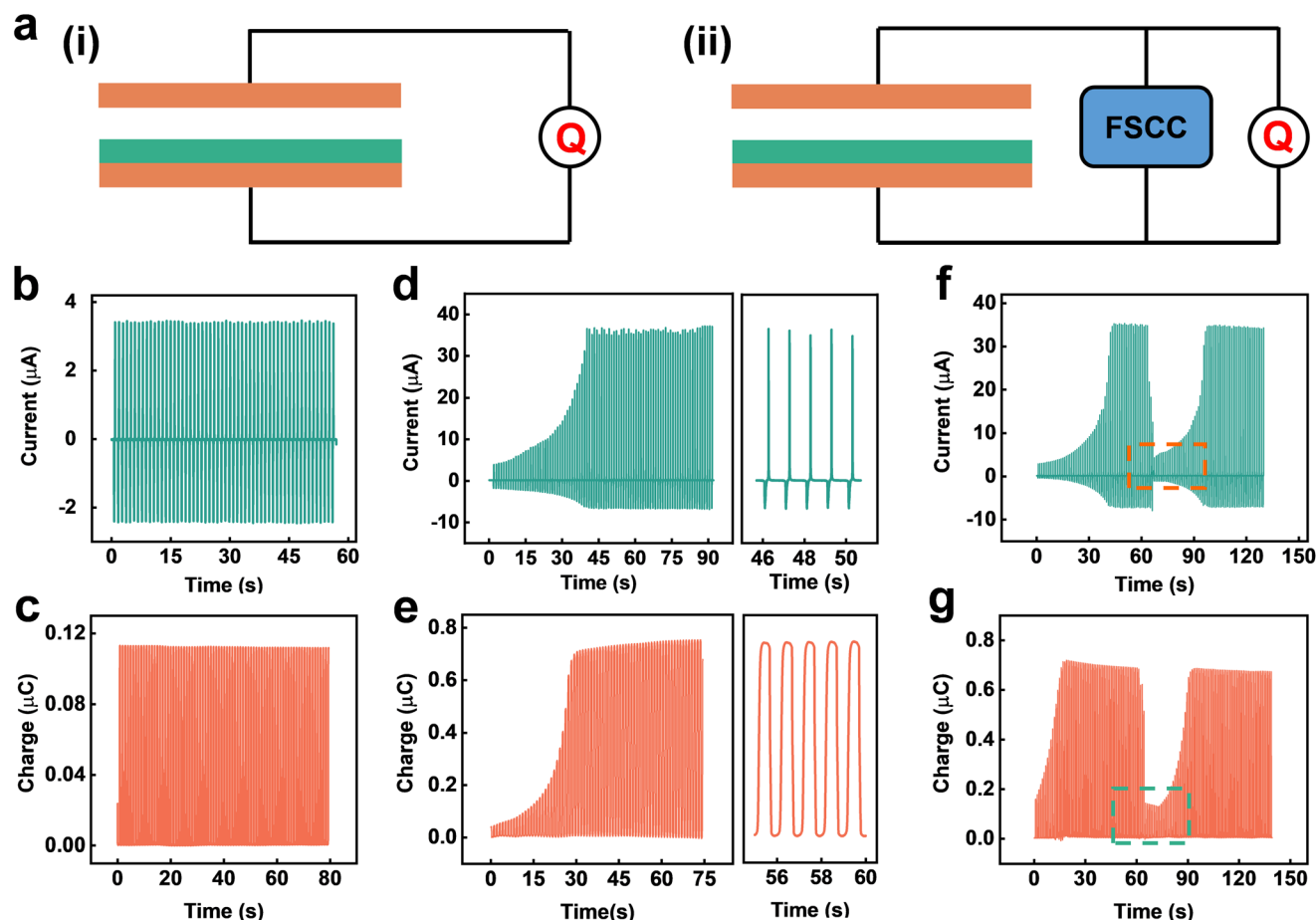
Fig. 2 Comparison of the output performance of the TENGs with and without charge excitation. (a) Circuit diagram of the TENG (i) without and (ii) with the charge excitation. (b) Short-circuit current and (c) transferred charge of the TENG without charge excitation. (d) Short-circuit current and (e) transferred charge of the FSC-TENG with matched voltage regulator diodes. (f) Short-circuit current and (g) transferred charge of the FSC-TENG when it is re-charged after discharging.

Subsequently, the effects of different parameters on the output performance of the FSC-TENG device under regular triggering were investigated, as shown in Fig. 3. ESI Table S1† shows the parameters of the electronic components used in this work. Because a large leakage current will bring great energy loss, especially in high-voltage applications, we tried choosing diodes with a small reverse leakage current. The relationship between the current/charge and withstand voltage of the rectifier diodes is shown in Fig. 3a and ESI Fig. S5a and b,† indicating that the short-circuit current and transferred charge both attain the maximum values at the withstand voltage of 800 V. The maximum short-circuit current and transferred charge arrive at 40.2 μA and 772.5 μC, respectively. Fig. 3b and ESI Fig. S5c and d† show that the short-circuit current and the transferred charge gradually increase when the capacitance of the adopted ceramic capacitors increases. The saturation values of current and charge rise from 16.6 μA and 591.4 nC (for 1 nF capacitor) to 41.7 μA and 778.0 μC (for 100 nF capacitor), respectively. Nevertheless, it takes more time to reach the charging saturation for larger capacitors, so the capacitors used in our FSC-TENG device are 22 nF. Fig. 3c

and ESI Fig. S5e and f† present the effect of the regulator diode number on the outputs. As the number of regulator diodes increases from 1 to 4, the short-circuit current and transferred charge both increase, but they both decrease upon further increasing the regulator diode number.

Besides the electronic component parameters, the influence of the external operating frequency on the electrical outputs of the FSC-TENG was investigated. When the frequency increases from 0.5 Hz to 2.0 Hz, the short-circuit current gradually increases, while the transferred charge possesses an optimum value of 752.4 nC at the frequency of 1 Hz, as shown in Fig. 3d and ESI Fig. S6.† The output current is nearly proportional to the frequency, reaching a maximum value of 43.7 μA at a frequency of 2 Hz. After optimizing the electronic component parameters, we also found that there exists a difference when these components are integrated on a breadboard or PCB. As shown in Fig. 3e and ESI Fig. S7,† the saturated current, and charge can increase from 34.0 μA and 633.0 nC (using the breadboard) to 36.5 μA and 752.4 nC (using the PCB), which may be due to the formation of many micro-capacitors by the metal foil on the breadboard. According to the above results,
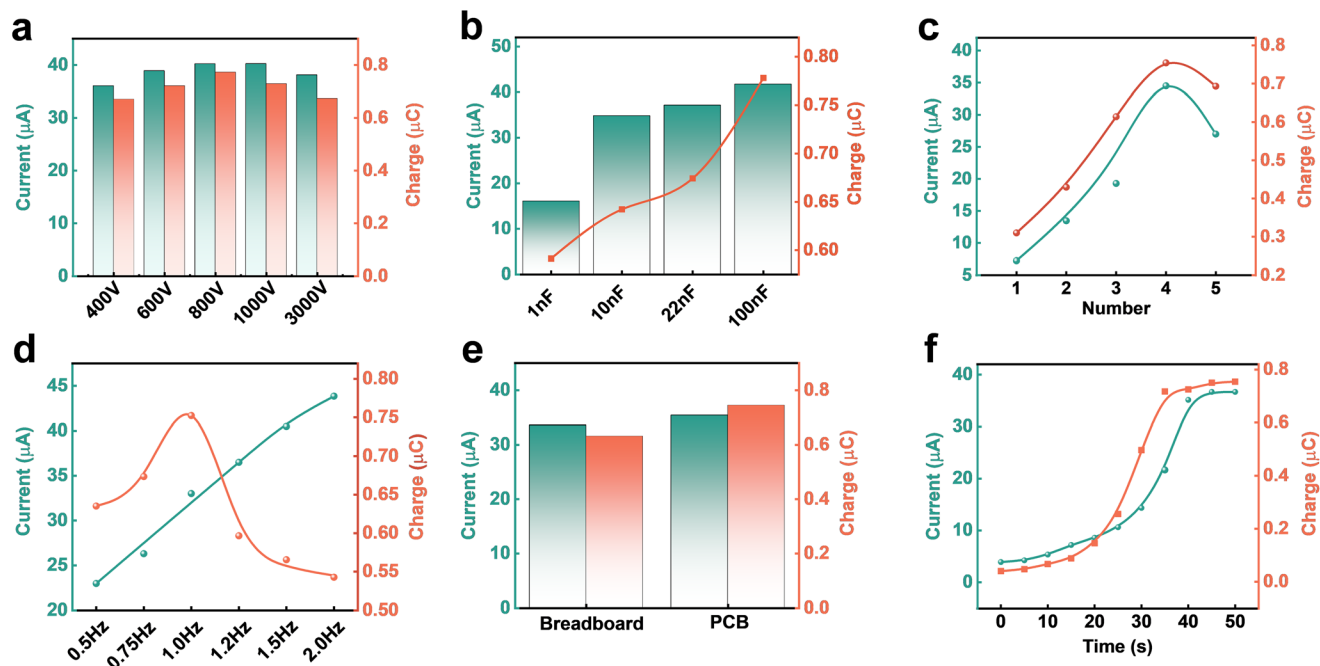
Fig. 3 Effects of different parameters on the TENG outputs. (a) Influence of the withstand voltage of the rectifier diodes on the short-circuit current and transferred charge of the FSC-TENG. (b) Short-circuit current and transferred charge of the FSC-TENG as functions of the capacitances of the ceramic capacitors. (c) Effect of the number of voltage regulator diodes on the short-circuit current and transferred charge. (d) Relationship between the current/charge and the external operating frequency. (e) Comparison of the current and transferred charge of the FSC-TENG when these components are integrated on a breadboard or PCB. (f) Short-circuit current and transferred charge curves of the FSC-TENG under optimal conditions.
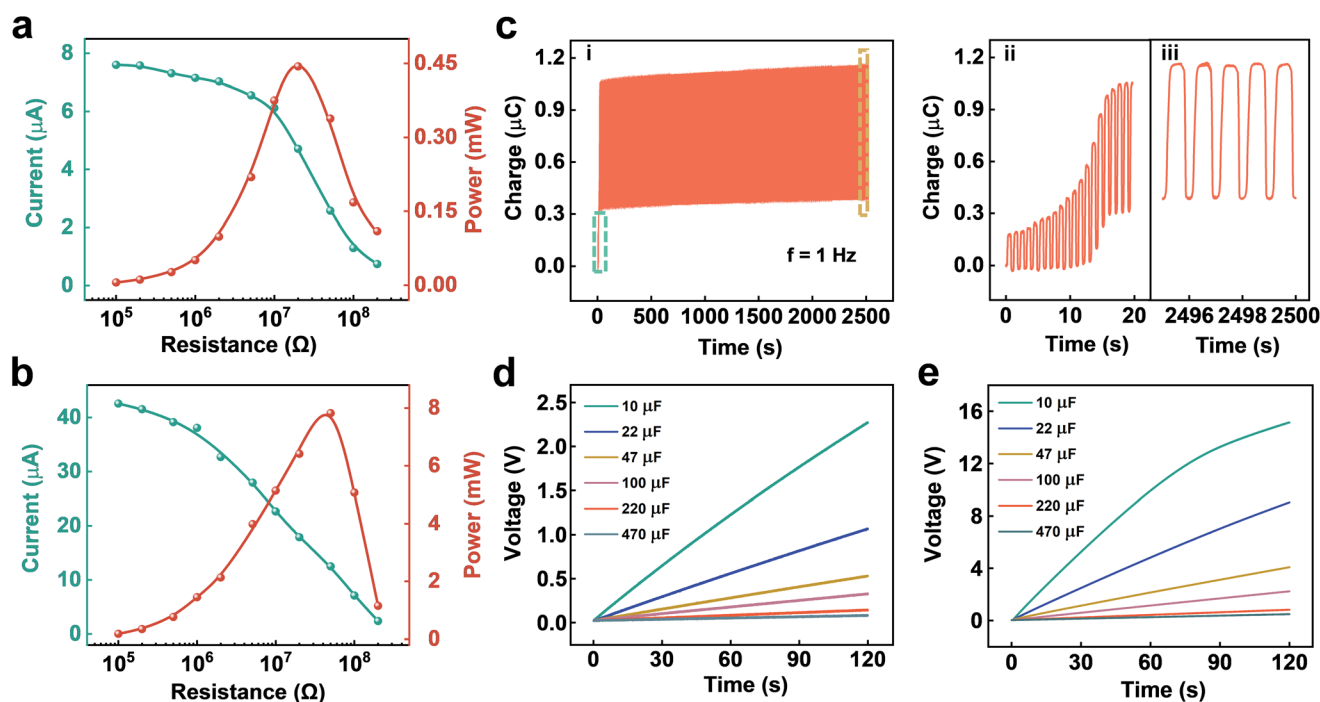

Fig. 4 Comparison of the performance of the FSC-TENG with a common TENG. (a and b) Output current and output power at different load resistances for the (a) common TENG, (b) FSC-TENG at 2 Hz. (c) (i) Stability profile of the output charge of the FSC-TENG at 1 Hz. (ii) Enlarged view of the output charge at the initial charging stage. (iii) Enlarged view of the output charge at the charge saturation stage. (d and e) Charging voltage on various capacitances for the (d) common TENG, (e) FSC-TENG.

the fractal structure charge-excitation circuit of 4 = 2 × 2, which consists of four Zener diodes of 150 V, nine rectifier diodes of 800 V, and four 22 nF ceramic capacitors, was chosen in the next experiments. Fig. 3f shows the profiles of short-circuit current and transferred charge of the FSC-TENG at the optimum conditions. The operating frequency was chosen as 1 Hz.

The resistive behavior of the FSC-TENG at the frequency of 2.0 Hz was studied and compared with the common TENG. As shown in Fig. 4a and b, when the load resistance increases from 0.1 MΩ to 200 MΩ, the current of the common TENG decreases from 7.6 µA to 0.7 µA, and a maximum power of 0.44 mW can be delivered at the matched resistance of 50 MΩ. In contrast, the current and power of the FSC-TENG arrived at 42.6 µA and 7.83 mW, respectively. The power has an enhancement of 16.8 times, and the matched resistance is still 50 MΩ. Fig. 4c(i) shows the variation process of the transferred charge for the FSC-TENG in 2500 s. Fig. 4c(ii) presents the enlarged view of the ongoing charge accumulation, and Fig. 4c(iii) represents the state of charge saturation. In addition, the charging capabilities of the TENG for different capacitors were compared between the two cases with and without charge exci-

tation. As shown in Fig. 4d and e, the charging voltage of a 10 µF capacitor reaches 2.3 V in 120 s for a common TENG, while the FSC-TENG can charge the capacitor to 15.2 V, with an improvement of 42.7 times in the stored energy. ESI Fig. S8† shows the charging profiles for different capacitors in the unsaturated state, and an enlarged view of the charging profiles during the charge excitation process is also shown. Both states demonstrate that the FSC-TENG can greatly increase the charging speed.

Finally, the practical applications of the FSC-TENG in our daily lives were demonstrated. Using the FSCC to manage the TENG for harvesting mechanical energy that could power some small portable electronic devices, through a mechanical switch and an energy storage capacitor, as shown in Fig. 5a. The FSCC contains nine rectifier diodes with a withstand voltage of 800 V, four regulator diodes of 150 V, four 10 nF ceramic capacitors, and an electrolytic capacitor. First, the FSC-TENG was employed to charge a 220 µF capacitor to drive a hygrothermograph under the regular triggering of a linear motor. When the voltage reaches 2.0 V, the hygrothermograph starts to work, and the temperature and humidity data are presented on the liquid crystal display screen. The charging and
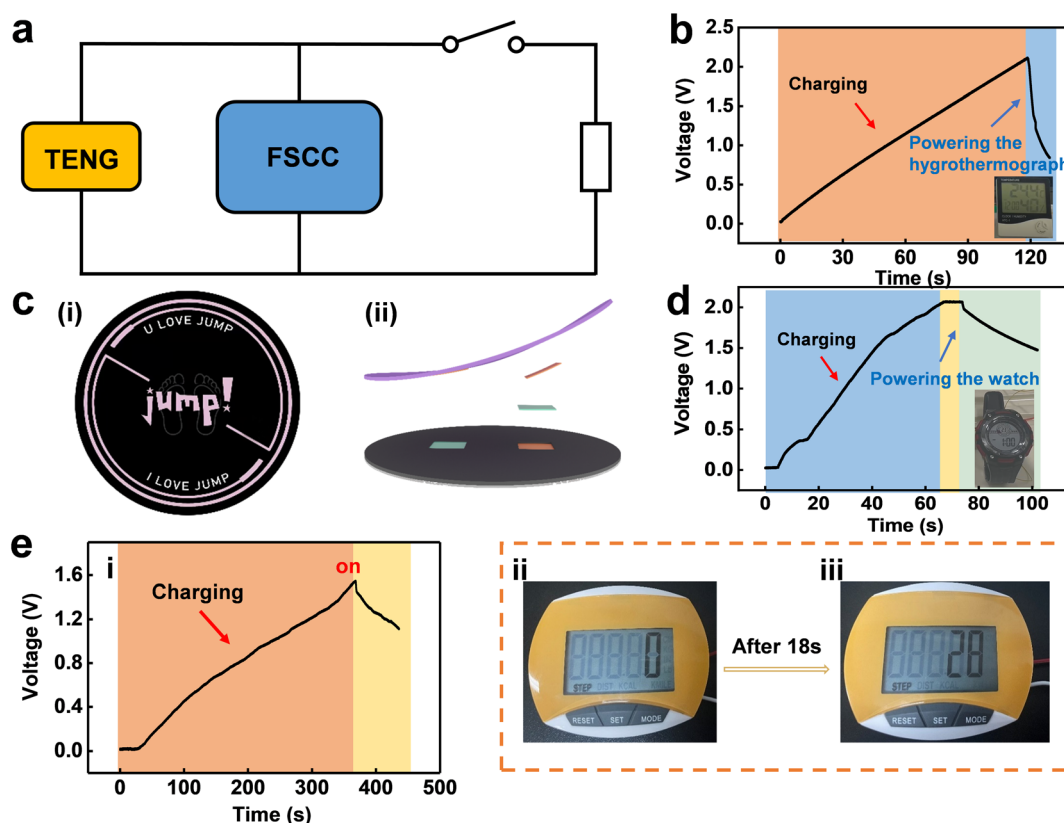

Fig. 5 Application demonstrations of the FSC-TENG in powering portable electronics. (a) Schematic diagram of the FSC-TENG for powering electronics through a mechanical switch and an energy storage capacitor. (b) Charging and discharging processes of a 220 µF capacitor when driving a hygrothermograph at 2 Hz. (c) Front view and sectional view of the yoga mat with the FSC-TENG. (d) Voltage profile on a 100 µF capacitor charged by the FSC-TENG integrated with the yoga mat to drive the electronic watch. (e) Photographs of the pedometer powered by the FSC-TENG below the yoga mat by charging a 470 µF capacitor after the exercise.

discharging processes of the capacitor to power the hygrothermograph is shown in Fig. 5b, and the experimental process is demonstrated in ESI Video S2.†

Nowadays, more and more people love sports, which are good for their physical and mental health. In this context, we tried to integrate our TENG device with a yoga mat to harvest the human-body motion energy. The device uses an acrylic plate with a 5 mm-thick sponge as the substrate, leaving two 100 mm × 100 mm grooves in the substrate, and the two TENGs placed in the grooves are connected to the FSCC. Fig. 5c shows the front views and sectional view of the yoga mat, and the photograph of the yoga mat integrated with the FSC-TENG is shown in ESI Fig. S9.† A capacitor of 100 μF was adopted to store the translated electrical energy for powering an electronic watch, as shown in Fig. 5d. After a person exercises on the yoga mat for 60 s, the voltage rises rapidly to 2.0 V, and the electronic watch starts to work. The watch can continue to work for 70 s after the stopping motion (ESI Video S3†), thus it can help the exerciser know the resting time. Another application demonstration is powering a pedometer by the FSC-TENG. During the exercising process, a 470 μF capacitor is charged to 1.5 V after 360 s, and the switch is turned on so that the pedometer is connected and works properly. Fig. 5e(ii) and (iii) shows the exerciser moves on 28 steps during 18 s. The charging and discharging processes of the capacitor to power the pedometer are shown in Fig. 5e, and the experimental process is demonstrated in ESI Video S4.† If we increase the number of FSC-TENGs to form an array, more output energy can be generated, and the charging time can be shortened.

Conclusion

In this work, a fractal charge-excitation circuit was developed to boost the output performance of the TENG. The electronic component parameters in the FSCC and external operating frequencies were optimized to achieve a better-boosting effect of TENG outputs. Under the optimal parameters, the FSC-TENG can deliver the maximum-transferred charge of 752.4 nC, which is nearly 5.8 times higher than that without charge excitation, and the power reaches the maximum value of 7.83 mW, which is enhanced by almost 16.8 times. The fractal structure and regulated diodes can facilitate generating high-density charge outputs and avoid dielectric breakdown. Furthermore, the FSC-TENG was employed to successfully drive a hygrothermograph and integrate it with a yoga mat to power an electronic watch and a pedometer, showing its great application potential. This work provides a platform for TENGs to achieve highly stable power generation using the charge excitation approach for daily applications.

Conflicts of interest

The authors declare no competing financial interest.

Acknowledgements

References

1 S. Chu and A. Majumdar, *Nature*, 2012, **488**, 294–303.
2 J. Chen and Z. L. Wang, *Joule*, 2017, **1**, 480–521.
3 Z. L. Wang, *Adv. Mater.*, 2012, **24**, 280–285.
4 H. Ouyang, Z. Liu, N. Li, B. Shi, Y. Zou, F. Xie, Y. Ma, Z. Li, H. Li, Q. Zheng, X. Qu, Y. Fan, Z. L. Wang, H. Zhang and Z. Li, *Nat. Commun.*, 2019, **10**, 1821.
5 S. Niu, N. Matsuhisa, L. Beker, J. Li, S. Wang, J. Wang, Y. Jiang, X. Yan, Y. Yun, W. Burnett, A. S. Y. Poon, J. B. H. Tok, X. Chen and Z. Bao, *Nat. Electron.*, 2019, **2**, 361–368.
6 D. Son, J. Kang, O. Vardoulis, Y. Kim, N. Matsuhisa, J. Y. Oh, J. W. To, J. Mun, T. Katsumata, Y. Liu, A. F. McGuire, M. Krason, F. Molina-Lopez, J. Ham, U. Kraft, Y. Lee, Y. Yun, J. B. Tok and Z. Bao, *Nat. Nanotechnol.*, 2018, **13**, 1057–1065.
7 L. Fogel and J. C. Kvedar, *npj Digital Med.*, 2018, **1**, 5.
8 Y. Lee, S. H. Cha, Y. W. Kim, D. Choi and J. Y. Sun, *Nat. Commun.*, 2018, **9**, 1804.
9 R. Cheng, C. Ning, P. Chen, F. Sheng, C. Wei, Y. Zhang, X. Peng, K. Dong and Z. L. Wang, *Adv. Energy Mater.*, 2022, **12**, 2201532.
10 C. Lu, J. Chen, T. Jiang, G. Gu, W. Tang and Z. L. Wang, *Adv. Mater. Technol.*, 2018, **3**, 1800021.
11 Y. Zi, S. Niu, J. Wang, Z. Wen, W. Tang and Z. L. Wang, *Nat. Commun.*, 2015, **6**, 8376.
12 S. Wang, L. Lin and Z. L. Wang, *Nano Energy*, 2015, **11**, 436–462.
13 V. J. Hodge, S. O'Keefe, M. Weeks and A. Moulds, *IEEE Trans. Intell. Transp. Syst.*, 2015, **16**, 1088–1106.
14 L. Zhang, S. X. Dou, H. K. Liu, Y. Huang and X. Hu, *Adv. Sci.*, 2016, **3**, 1600115.
15 J. Han, X. Yang, L. Liao, G. Zhou, G. Wang, C. Xu, W. Hu, M. E. R. Debora and Q. Song, *Nano Energy*, 2019, **58**, 331–337.
16 L. Long, W. Liu, Z. Wang, W. He, G. Li, Q. Tang, H. Guo, X. Pu, Y. Liu and C. Hu, *Nat. Commun.*, 2021, **12**, 4689.
17 C. Shan, W. Liu, Z. Wang, X. Pu, W. He, Q. Tang, S. Fu, G. Li, L. Long, H. Guo, J. Sun, A. Liu and C. Hu, *Energy Environ. Sci.*, 2021, **14**, 5395–5405.
18 Z. L. Wang, J. Chen and L. Lin, *Energy Environ. Sci.*, 2015, **8**, 2250–2282.
19 Z. L. Wang, *Adv. Energy Mater.*, 2020, **10**, 2000137.
20 J. Wang, Z. Wen, Y. Zi, P. Zhou, J. Lin, H. Guo, Y. Xu and Z. L. Wang, *Adv. Funct. Mater.*, 2016, **26**, 1070–1076.

21 J. Chen, Y. Huang, N. Zhang, H. Zou, R. Liu, C. Tao, X. Fan and Z. L. Wang, *Nat. Energy*, 2016, **1**, 16138.

22 P. K. Yang, L. Lin, F. Yi, X. Li, K. C. Pradel, Y. Zi, C. I. Wu, J. H. He, Y. Zhang and Z. L. Wang, *Adv. Mater.*, 2015, **27**, 3817–3824.

23 P. K. Yang, Z. H. Lin, K. C. Pradel, L. Lin, X. Li, X. Wen, J. H. He and Z. L. Wang, *ACS Nano*, 2015, **9**, 901–907.

24 C. Wu, A. C. Wang, W. Ding, H. Guo and Z. L. Wang, *Adv. Energy Mater.*, 2019, **9**, 1802892.

25 Y. Yang, X. Guo, M. Zhu, Z. Sun, Z. Zhang, T. He and C. Lee, *Adv. Energy Mater.*, 2022, **18**, 2203040.

26 A. Haroun, X. Le, S. Gao, B. Dong, T. He, Z. Zhang, F. Wen, S. Xu and C. Lee, *Nano Express*, 2021, **2**, 022005.

27 J. Zhu, H. Wang, Z. Zhang, Z. Ren, Q. Shi, W. Liu and C. Lee, *Nano Energy*, 2020, **73**, 104760.

28 J. Wang, L. Pan, H. Guo, B. Zhang, R. Zhang, Z. Wu, C. Wu, L. Yang, R. Liao and Z. L. Wang, *Adv. Energy Mater.*, 2019, **9**, 1802906.

29 L. Xu, T. Z. Bu, X. D. Yang, C. Zhang and Z. L. Wang, *Nano Energy*, 2018, **49**, 625–633.

30 Z. Yang, Y. Yang, H. Wang, F. Liu, Y. Lu, L. Ji, Z. L. Wang and J. Cheng, *Adv. Energy Mater.*, 2021, **11**, 2101147.

31 H. Wang, L. Xu, Y. Bai and Z. L. Wang, *Nat. Commun.*, 2020, **11**, 4203.

32 G. Li, S. Fu, C. Luo, P. Wang, Y. Du, Y. Tang, Z. Wang, W. He, W. Liu, H. Guo, J. Chen and C. Hu, *Nano Energy*, 2022, **96**, 107068.

33 W. Liu, Z. Wang, G. Wang, G. Liu, J. Chen, X. Pu, Y. Xi, X. Wang, H. Guo, C. Hu and Z. L. Wang, *Nat. Commun.*, 2019, **10**, 1426.

34 H. Wang, J. Zhu, T. He, Z. Zhang and C. Lee, *Nano Energy*, 2020, **78**, 105241.

35 J. Zhu, Z. Sun, J. Xu, R. D. Walczak, J. A. Dziuban and C. Lee, *Sci. Bull.*, 2021, **66**, 1176–1185.

36 W. Liu, Z. Wang, G. Wang, Q. Zeng, W. He, L. Liu, X. Wang, Y. Xi, H. Guo, C. Hu and Z. L. Wang, *Nat. Commun.*, 2020, **11**, 1883.